A Decentralized Current-Sharing Controller Endows Fast Transient Response to Parallel DC–DC Converters

Haojie Wang, *Student Member, IEEE*, Minxiao Han, Renke Han, *Student Member, IEEE*, Josep M. Guerrero, *Fellow, IEEE*, and Juan C. Vasquez, *Senior Member, IEEE*

***Abstract*—This paper proposes a decentralized current-sharing control strategy to endow fast transient response to paralleled dc–dc converters systems, such as dc microgrids or distributed power systems. The proposed controller consist of two main control loops: an external voltage droop control for current-sharing proposes and an internal current loop. The external droop control loop is designed as a voltage loop with embedded virtual impedance, which avoids the use of a slow voltage loop and a separate extra virtual impedance loop that may limit the system bandwidth. The internal current loop, thanks to the external control loop simplification, plays a major role in the system bandwidth, so that an adaptive proportional-integral (PI) controller is proposed for this matter. In the paper, two different droop control methods have been modeling, designed, simulated, and tested: The conventional virtual-impedance-loop based *V–I* droop and the proposed embedded-virtual-impedance based *I–V* droop. In order to compare the dynamic response performances between two droop controllers, their state-space models have been developed and analyzed in this paper. The results show that the dynamic response of the *I–V* droop control is faster than that of the conventional *V–I* droop control. Furthermore, by analyzing the effects from *I–V* droop control parameters, the errors can be reduced faster by enlarging the proportional terms, but with no fluctuations, and then completely eliminated by restoring back to small proportional values. Meanwhile, there exists a tradeoff phenomenon between the fast dynamic response and good steady-state performance; thus, an adaptive PI controller is proposed to both improve dynamic response and guarantee good steady-state performance simultaneously. Experimental results are shown to verify the accuracy of the models and the effectiveness of the proposed control framework.**

***Index Terms*—Adaptive PI control, droop control, dynamic response, large-signal model, paralleled dc–dc converters.**

I. Introduction

THE concept of dc microgrid (MG) provides a promising solution to integrate renewable energy sources into the power grid [1]–[3]. In an islanded dc MG, energy storage system (ESS) need to be installed in the system to provide the voltage support and guarantee the stable operation [4]–[6]. Due to the capacity extending and distributed configuration of dc MG, multibatteries are usually connected to the common bus by using paralleled converters [7], [8]. Another application for multiple dc–dc converters connected in parallel giving voltage support and current-sharing at the same time, are the distributed power systems (DPS). In a DPS, a number of multiple busses with different voltages are interconnected by multiple paralleled dc–dc converters.

In the aforementioned applications, the droop control is often used by imposing virtual resistance (VR) in order to achieve autonomous (communicationless) current sharing among paralleled converters [9]–[11]. When using droop control methods, also named primary control, the major concern of previous works are focused on the secondary and tertiary control levels inside the hierarchical control structure according to voltage deviations caused by line impedance [12]–[16], state of charge for battery management systems [17]–[19], power losses [19]–[22], and communication algorithms [16], [22], [23]. Major part of those methods are based on an adaptive droop control with the virtual impedance or the voltage reference able to adjust those values according to the signals sent by the superior control levels (secondary/tertiary). However, the dynamical process of the droop control to reach a new steady-state operation point has not been studied so much in previous works. Slow response performance can elongate the recovery time of voltage and current, which has adverse effect on the power quality of the system. In addition, due to the load and generation power flows, converters output currents oscillations may exist when dynamic response performances are poor and, thus, bus voltage fluctuations may attempt system stability [24].

For the improvement of dynamic characteristics of ac MGs, a small signal state-space model of the whole MG including the droop controller, network, and loads is proposed in [25], and the root locus method is used to analyze the dynamic characteristics. On the other hand, the dynamic characteristics of a current-fed converter developed from the corresponding voltage-fed converter by applying the duality-transformation method are investigated in [26], which is based on the photovoltaic generator. In [27], a feed-forward control based on dual-loop constant voltage PI control for three-phase interleaved dc–dc converter in dc

Manuscript received January 5, 2017; revised April 9, 2017; accepted May 31, 2017. Date of publication June 12, 2017; date of current version February 1, 2018. This work was supported by the Science and Technology Project of State Grid (PDB17201600116). Recommended for publication by Associate Editor Y. Li. *(Corresponding author: Haojie Wang.)*

H. Wang and M. Han are with the School of Electric and Electronic Engineering, North China Electric Power University, Beijing 102206, China (e-mail: bjwanghaojie@163.com; hanminxiao@263.net).

R. Han, J. M. Guerrero, and J. C. Vasquez are with the Department of Energy Technology, Aalborg University, Aalborg 9220, Denmark (e-mail: rha@et.aau.dk; joz@et.aau.dk; juq@et.aau.dk).

Color versions of one or more of the figures in this paper are available online at http://ieeexplore.ieee.org.

Digital Object Identifier 10.1109/TPEL.2017.2714342

MG is proposed, which is used to increase the output current reference of the converter when a load change occurs; then, the response speed can be improved, but this method is applicable to dc MG that has only one dc–dc converter. In addition, until now there are no reports dealing with the comparison of dynamic response performances between the different droop controls. To fill this gap, this paper presents a comparison of dynamic response performances between two droop control methods, named *V–I* and *I–V* droop controllers, showing that the dynamic response of the *I–V* droop control is faster.

In order to analyze the dynamic response performances of the two droop control methods, mathematic models need to be first built. As a typical method, average-value modeling for converters has been studied in many publications [28], [29]. Average-value modeling method, whose objective is to replace the discontinuous switching cells with continuous blocks that represent the averaged behavior of the switching cell within a prototypical switching interval, can be derived using state-space averaging or circuit averaging methods [30]–[32]. Considering the inductor-diode-MOSFET switching cell as a simplified variable current source feeding output *RC* circuit, a model is proposed based on the average injected inductor current in [33]. In [34], instead of using traditional small or linear ripple approximations the model is developed by using the correction coefficients that can account for the current and voltage nonlinear waveforms. The concept of input–output stability is applied to estimate the large-signal stability region via the small-signal feedback control loops in [35], by which the effect of the small-signal loop gains on the large-signal stability region can be also revealed. In this paper, based on the average-value modeling theory, the state-space models of the two droop controls for the analysis of the dynamic characteristics are built. The variation of the load current is set as the input of the model, so that the relations of all the variables in the model are linear. The state variables of the model include the variations of converter's output current and bus voltage caused by load changes, so that the model can be used to analyze the dynamic response performances of the system. This model has universal applicability for the analysis of dynamic process from one to another steady-state condition for paralleled dc–dc converters.

Although the *I–V* droop controller is faster than the *V–I* droop controller, this paper investigates whether there is a room for the further improvement of the *I–V* droop control transient response, and a novel adaptive PI control is proposed according to the analysis. Chen *et al.* [36] propose a parameter tuning algorithm to enable an adaptive PI controller to learn to control a changing process by merely observing the process output errors, which is devised to guarantee the stability of the system. In [37], the adaptive PI controllers are used for the current and voltage control loops of three phase ac–dc pulse width modulation converter by automatically adjusting PI control gains via the current and voltage error signals to improve the converters' tracking performance. In [38], a stable adaptive PI control is designed for the output voltage regulation of a quadratic boost converter, and the identification of a large class of converters that can be stabilized via adaptive PI control is the main contribution. Since abrupt changes of proportional parameters of current PI controllers have adverse effects on the dynamic performances of paralleled dc–dc converters, in this paper, a compensate term is added into the output duty ratio, which is indispensable for the realization of the proposed adaptive PI control.

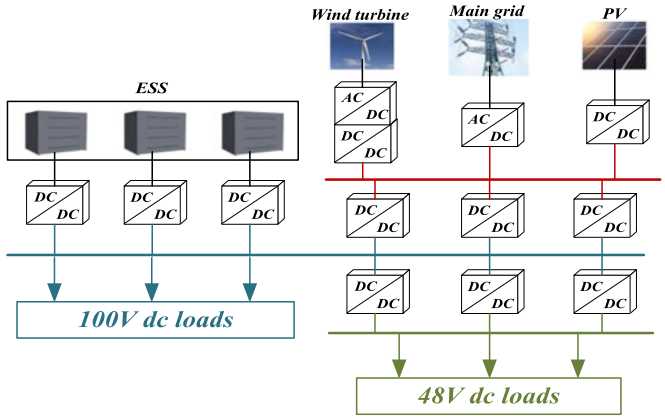

Fig. 1. Typical structure of dc MG.

This paper presents a comparison of dynamic response performances between the *V–I* and *I–V* droop controllers. When a load change occurs, the dynamical process to reach a new steady-state point is analyzed and improved. First, the modeling method, which is used for the dynamic analysis of the two droop controllers, is proposed. Second, the root locus methods are used to compare the dynamic response performances between the two droop controllers. The proposed models and the comparative analysis are verified by means of experimental results. Third, the influence of *I–V* droop control parameters on the dynamic response performances is analyzed and a novel adaptive PI controller is proposed to further improve its dynamic response performances. Finally, experiments are performed to verify the proposed control.

This paper is structured as follows. In Section II, the models of the two droop controllers are built. In Section III, the comparison of dynamic response performances between two droop control methods is presented and verified by experiments. In Section IV, the adaptive PI control to improve the dynamic response of *I–V* droop control is proposed and verified by experiments. Section V concludes this paper.

II. Modeling for Two Droop Control Schemes

A typical structure of a dc MG consisted of paralleled dc–dc converters with multiple ESS is shown in Fig. 1. The ESS can support the bus voltage by using droop control on islanded operation mode. The *V–I* droop control method for paralleled dc–dc converters is achieved by linearly reducing the voltage reference when the output current increases as shown in Fig. 2(a). In this method, also known as VR loop, the voltage reference can be obtained by emulating a droop characteristic as

$$u_{\mathrm{ref}} = U_{\mathrm{rate}} - ri \tag{1}$$

where u_{ref} is the voltage reference, U_{rate} is the no load voltage of the source, r is the VR, and i is the average inductor current

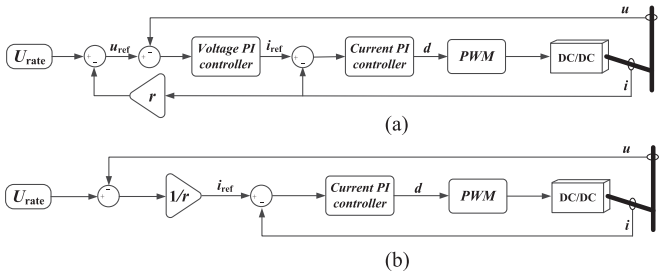

Fig. 2. Control diagrams of two droop control implementations. (a) *V–I* droop control. (b) *I–V* droop control.

(namely the output current). By reversing the reference output from the droop characteristic, the *I–V* droop control can be obtained as shown in Fig. 2(b), which is achieved by linearly increasing the current reference when the bus voltage decreases. The current reference can be computed as

$$i_{\rm ref} = \frac{1}{r}\left(U_{\rm rate} - u\right) \tag{2}$$

where $i_{\rm ref}$ is the current reference and *u* is the bus voltage. For *n* paralleled dc–dc converters based on either droop control, the total load current can be shared by converters in proportion to their reciprocals of VRs at steady state:

$$i_1 r_1 = i_2 r_2 = \cdots = i_n r_n \tag{3}$$

where $i_k\,(k = 1, 2, \ldots, n)$ is the output current, $r_k\,(k = 1, 2, \ldots, n)$ is the VR, and n is the number of parallel-connected converters.

A. Modeling for V–I Droop Control

According to the average-value modeling theory, the increment of the average inductor current in any arbitrary switching cycle can be obtained as [23]

$$\Delta i_{\rm cycle} = \int_0^T \frac{dU_{\rm in} - u_{\rm dc}}{L} dt \tag{4}$$

where $\Delta i_{\rm cycle}$ is the increment of the average inductor current in an arbitrary switching cycle, L is the inductance value, T is the switching cycle, $U_{\rm in}$ is the input voltage, d is the duty ratio of the upper bridge arm, and $u_{\rm dc}$ is the dc bus voltage.

In steady state, let u_0 represent the bus voltage, $i_{\rm ld0}$ represent the load current, $u_{\rm ref0}$, $i_{\rm ref0}$, i_0, and d_0 represent the voltage reference of the voltage PI controller, the current reference of current PI controller, the average inductor current, and the duty ratio, respectively. Setting zero-time as the instant of a load changing, suppose that the variation of load current is $i_{\rm ldv}(t)$. After a load variation, let $u_d(t)$ represent the variation of dc bus, $u_{d\rm ref}(t)$, $i_{d\rm ref}(t)$, $i_d(t)$, and $d_d(t)$ represent the variation of voltage reference, current reference, average inductor current, and duty ratio, respectively. Considering the variation of the average inductor current, (4) can be written as

$$i_d(t) = \int_0^t \frac{\left[d_0 + d_d(t)\right] U_{\rm in} - \left[u_0 + u_d(t)\right]}{L} dt. \tag{5}$$

According to (4), the following equation can also be obtained as

$$d_0 = \frac{u_0}{U_{\rm in}}. \tag{6}$$

By substituting (6) into (5) and calculating its time derivative, (5) can be rewritten as

$$\frac{di_d(t)}{dt} = \frac{d_d(t)U_{\rm in} - u_d(t)}{L}. \tag{7}$$

In addition, since $i_{\rm ld0} = i_0$ at steady state, the following equation can be obtained as

$$\begin{aligned}\frac{d\left[u_0 + u_d(t)\right]}{dt} &= \frac{du_d(t)}{dt} \\ &= \frac{i_0 + i_d(t) - i_{\rm ld0} - i_{\rm ldv}(t)}{C} = \frac{i_d(t) - i_{\rm ldv}(t)}{C}\end{aligned} \tag{8}$$

where *C* is the dc bus capacitance. According to (1), at steady state, the voltage reference can be obtained as

$$u_{\rm ref0} = u_0 = U_{\rm rate} - r i_0. \tag{9}$$

And expressed in the same form, considering steady-state values and variations:

$$u_{\rm ref0} + u_{d\rm ref}(t) = U_{\rm rate} - r[i_0 + i_d(t)]. \tag{10}$$

Let $k_{\rm pu}$ and $k_{\rm iu}$ represent the proportional and integral terms of the voltage PI controller, respectively, so that the increment of the current reference can be computed as

$$\begin{aligned}i_{d\rm ref}(t) = {} & k_{\rm pu}\left\{\left[u_{\rm ref0} + u_{d\rm ref}(t)\right] - \left[u_0 + u_d(t)\right]\right\} \\ & + k_{\rm iu}\int_0^t \left\{\left[u_{\rm ref0} + u_{d\rm ref}(t)\right] - \left[u_0 + u_d(t)\right]\right\} dt.\end{aligned} \tag{11}$$

Calculating the time derivative of (11) and by considering (7)–(10); then, (11) can be rewritten as

$$\begin{aligned}\frac{di_{d\rm ref}(t)}{dt} = {} & -\left(\frac{k_{\rm pu}}{C} + r k_{\rm iu}\right) i_d(t) - \frac{r k_{\rm pu} U_{\rm in}}{L} d_d(t) \\ & + \left(\frac{r k_{\rm pu}}{L} - k_{\rm iu}\right) u_d(t) + \frac{k_{\rm pu}}{C} i_{\rm ldv}(t).\end{aligned} \tag{12}$$

Let $k_{\rm pi}$ and $k_{\rm ii}$ represent the proportion and integral terms of current PI controller, respectively, so that the increment of duty ratio can be computed as

$$\begin{aligned}d_d(t) = {} & k_{\rm pi}\left\{\left[i_{\rm ref0} + i_{d\rm ref}(t)\right] - \left[i_0 + i_d(t)\right]\right\} \\ & + k_{\rm ii}\int_0^t \left\{\left[i_{\rm ref0} + i_{d\rm ref}(t)\right] - \left[i_0 + i_d(t)\right]\right\} dt.\end{aligned} \tag{13}$$

In steady state, $i_{\rm ref0} = i_0$, so that calculating the time derivative of (13) and by considering (7) and (12); then, (13) can be

rewritten as

$$\begin{aligned}\frac{dd_d(t)}{dt} = &-\left(\frac{k_{\rm pi}k_{\rm pu}}{C}+rk_{\rm pi}k_{\rm iu}+k_{\rm ii}\right)i_d(t)\\ &-\frac{rk_{\rm pi}k_{\rm pu}E+k_{\rm pi}U_{\rm in}}{L}d_d(t)\\ &+\left(\frac{rk_{\rm pi}k_{\rm pu}+k_{\rm pi}}{L}-k_{\rm pi}k_{\rm iu}\right)u_d(t)\\ &+k_{\rm ii}i_{d\rm ref}(t)+\frac{k_{\rm pi}k_{\rm pu}}{C}i_{\rm ldv}(t). \end{aligned}\tag{14}$$

Thus, (7), (8), (12), and (14) can be rewritten in a state-space model as the following compact form: Equation (15) as shown at the bottom of the page.

B. Modeling for I–V Droop Control

Let $i_{\rm ref0}, i_0$ and d_0 represent the current reference, the average inductor current, and the duty ratio in steady state, $i_{d\rm ref}(t), i_d(t)$, and $d_d(t)$ represent the variation of current reference, inductor current, and duty ratio after load changing. According to (2), at steady state, the current reference can be obtained as

$$i_{\rm ref0}=i_0=\frac{1}{r}\left(U_{\rm rate}-u_0\right).\tag{16}$$

And expressed in the same form, considering steady-state values and variations:

$$i_{\rm ref0}+i_{d\rm ref}(t)=\frac{1}{r}\left\{U_{\rm rate}-\left[u_0+u_d(t)\right]\right\}.\tag{17}$$

Calculating the time derivative of (13) and considering (16) and (17), (13) can be rewritten as

$$\frac{dd_d(t)}{dt}=k_{\rm pi}\left[-\frac{du_d(t)}{rdt}-\frac{di_d(t)}{dt}\right]+k_{\rm ii}\left[-\frac{u_d(t)}{r}-i_d(t)\right].\tag{18}$$

Substituting (7) and (8) into (18), (18) can be rewritten as

$$\begin{aligned}\frac{dd_d(t)}{dt} = &-\left(\frac{k_{\rm pi}}{rC}+k_{\rm ii}\right)i_d(t)+\left(\frac{k_{\rm pi}}{L}-\frac{k_{\rm ii}}{r}\right)u_d(t)\\ &-\frac{k_{\rm pi}U_{\rm in}}{L}d_d(t)+\frac{k_{\rm pi}}{rC}i_{\rm ldv}(t).\end{aligned}\tag{19}$$

TABLE I
PARAMETERS FOR COMPARISON BETWEEN TWO DROOP CONTROLLERS

	Parameters		Value
	Symbol	Description	
Electric setup parameters	$U_{\rm in}$	Input voltage	230 V
	L	Converter inductance	1.8 mH
	C	DC bus capacitance	2200 μF
Control parameters	r	VR	1 Ω
	$k_{\rm pi}$	Current loop proportional term	0.001
	$k_{\rm ii}$	Current loop integral term	0.01
	$U_{\rm rate}$	Rated bus voltage	100 V

Then (7), (8), and (19) can be rewritten in a state-space model as the following compact form:

$$\begin{bmatrix}\dot i_d\\ \dot d_d\\ \dot u_d\end{bmatrix}=\begin{bmatrix}0 & \frac{U_{\rm in}}{L} & -\frac{1}{L}\\ -\left(\frac{k_{\rm pi}}{rC}+k_{\rm ii}\right) & -\frac{k_{\rm pi}U_{\rm in}}{L} & \frac{k_{\rm pi}}{L}-\frac{k_{\rm ii}}{r}\\ \frac{1}{C} & 0 & 0\end{bmatrix}\cdot\begin{bmatrix}i_d\\ d_d\\ u_d\end{bmatrix}+\begin{bmatrix}0\\ \frac{k_{\rm pi}}{rC}\\ -\frac{1}{C}\end{bmatrix}\cdot i_{\rm ldv}.\tag{20}$$

III. DYNAMIC ANALYSIS FOR TWO DROOP SCHEMES

A. Dynamics Comparison for the Two Droop Controllers

By setting the average inductor current as the output, the root locus method has been employed to analyze the dynamic characteristics of the *V–I* and *I–V* droop controls. The parameters of electrical setup, current PI controller, and VR of the two controls are listed in Table I. Setting the voltage loop integral parameter of the *V–I* droop control as 1 and by changing its proportional term value from 0.01 to 1, the pole shifting trajectories of the output current are shown in Fig. 3. Setting the voltage loop proportional term value of the *V–I* droop control as 0.1 and by changing its integral term value from 0.1 to 10, the pole shifting trajectories of the output current are shown in Fig. 4.

From the pole shifting trajectories of two droop controls it can be seen that during the dynamical process, higher frequency

$$\begin{bmatrix}\dot i_d\\ \dot i_{d\rm ref}\\ \dot d_d\\ \dot u_d\end{bmatrix}=\begin{bmatrix}0 & 0 & \frac{U_{\rm in}}{L} & -\frac{1}{L}\\ -\left(\frac{k_{\rm pu}}{C}+rk_{\rm iu}\right) & 0 & -\frac{rk_{\rm pu}U_{\rm in}}{L} & \frac{rk_{\rm pu}}{L}-k_{\rm iu}\\ -\left(\frac{k_{\rm pi}k_{\rm pu}}{C}+rk_{\rm pi}k_{\rm iu}+k_{\rm ii}\right) & k_{\rm ii} & -\frac{rk_{\rm pi}k_{\rm pu}U_{\rm in}+k_{\rm pi}U_{\rm in}}{L} & \frac{rk_{\rm pi}k_{\rm pu}+k_{\rm pi}}{L}-k_{\rm pi}k_{\rm iu}\\ \frac{1}{C} & 0 & 0 & 0\end{bmatrix}\cdot\begin{bmatrix}i_d\\ i_{d\rm ref}\\ d_d\\ u_d\end{bmatrix}+\begin{bmatrix}0\\ \frac{k_{\rm pu}}{C}\\ \frac{k_{\rm pi}k_{\rm pu}}{C}\\ -\frac{1}{C}\end{bmatrix}\cdot i_{\rm ldv}.\tag{15}$$

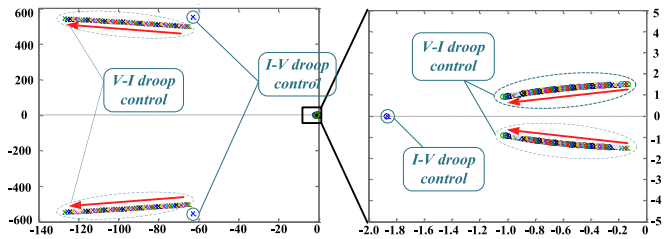

Fig. 3. Pole shifting trajectories of two controls with outer loop proportional term of *V–I* droop control shifting.

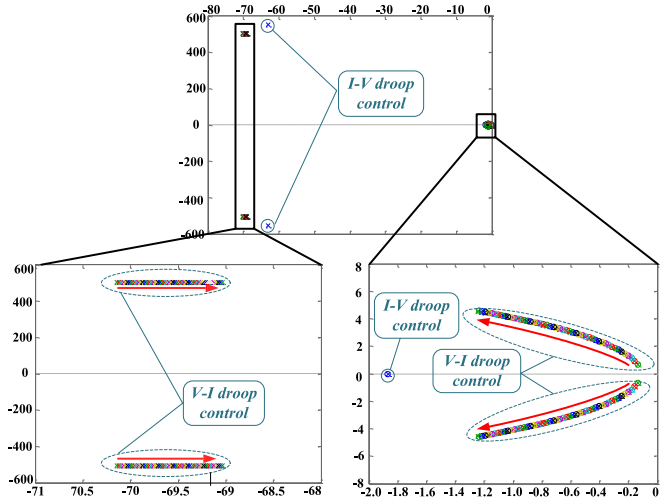

Fig. 4. Pole shifting trajectories of two controls with outer loop integral term of *V–I* droop control shifting.

oscillation can be caused by both the two droop controls, which attenuates rapidly. The low-frequency oscillation that attenuates much more slowly can be caused by the *V–I* droop control due to the two poles closer to imaginary axis no matter how much the voltage loop parameters are.

The comparison between the two droop controls shows that when the system current is changed due to either generation or consumption, the system with the *I–V* droop control will reach steady state more rapidly compared with the *V–I* droop controller, so that the dynamic response of the *I–V* droop control is faster.

B. Verification for Model and Analysis

The islanded experimental dc MG setup, which consists of four 0.7-kW dc–dc converters, a battery, a real-time dSPACE1006 platform, and resistance loads, has been built as shown in Fig. 5. The switching frequency is set to 10 kHz. The parameters of electrical setup, current PI controller, and VR of the two droop controls are listed in Table I as well. The proportional and integral term values of the voltage PI controller are set as 0.1 and 1, respectively. The tests of step response for output current based on *V–I* droop control and *I–V* droop control have been obtained by using the obtained models and contrasted with the experimental results.

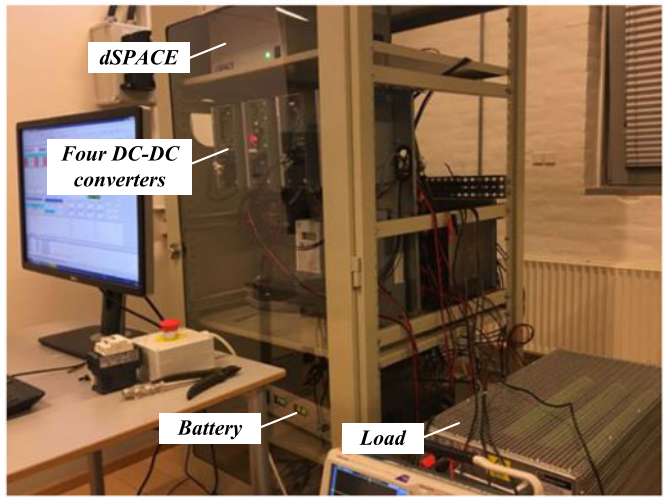

Fig. 5. Islanded dc MG experimental platform.

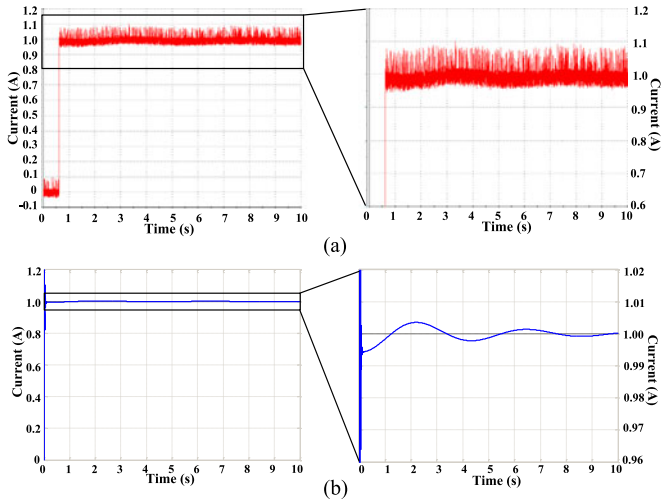

Fig. 6. Step response waveform of the output current by using *V–I* droop control. (a) Experimental result. (b) Model.

Putting into 100-W load, the experimental waveform of the output current obtained by using the *V–I* droop control is shown in Fig. 6(a), which is identical with that from the model, as shown in Fig. 6(b). Fig. 7(a) shows the experimental waveform of the output current obtained by using *I–V* droop control, which is identical with that from the model as shown in Fig. 7(b). It can be seen that the models are accurate and the low-frequency fluctuation attenuating much slowly can be caused by the *V–I* droop control, cannot be obtained by using the *I–V* droop control, which is consistent with the analysis.

IV. Adaptive PI Control and Experiment Verification

Section III has shown that the dynamic response performance of the *I–V* droop control is faster than that of the *V–I* droop control. However, the dynamic response performance of *I–V* droop control can be influenced by other factors as well. According to the state-space model, it can be found that the factors influencing

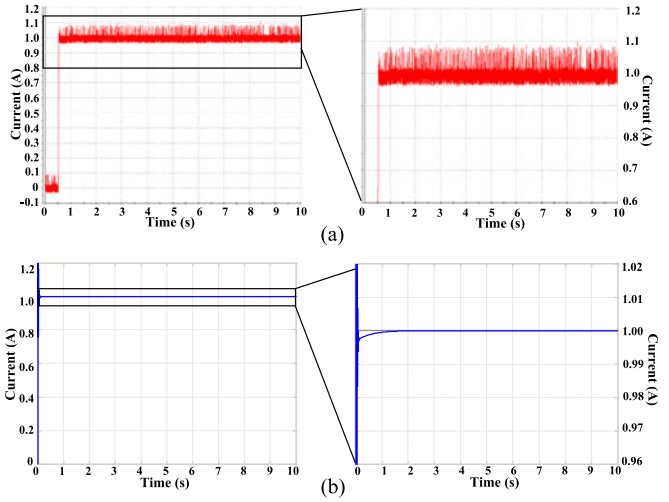

Fig. 7. Step response waveform of the output current by using *I–V* droop control. (a) Experimental result. (b) Model.

the dynamic performance of the *I–V* droop control include the input voltage, the converter inductance, the bus capacitance, the VR, and the proportional and integral parameters of current PI controller. However, the VR and the electrical setup parameters can hardly be changed, so it is more practical to improve the dynamic characteristics by adjusting PI controller parameters, which will be further studied in this section.

A. Analysis of the Dynamic Response Performance

For n dc–dc converters, let $\boldsymbol{I}_d$ and $\boldsymbol{D}_d$ represent the variations of the average inductor currents and the duty ratios, respectively, where

$$\boldsymbol{I}_d = \begin{bmatrix} i_{d1} & i_{d2} & \cdots & i_{dn} \end{bmatrix}, \ \boldsymbol{D}_d = \begin{bmatrix} d_{d1} & d_{d2} & \cdots & d_{dn} \end{bmatrix}.$$

Let $\boldsymbol{I}$ represent the n-order vector with all elements 1. Since all the modules share the common part of capacitor and load, (7) and (8) can be, respectively, rewritten as

$$\frac{\boldsymbol{dI}_d(\boldsymbol{t})}{\boldsymbol{t}} = [\boldsymbol{D}_d(\boldsymbol{t})\boldsymbol{U}_{\mathbf{in}} - u_d(t)\boldsymbol{I}]\boldsymbol{L}^{-1} \tag{21}$$

$$\frac{du_d(t)}{dt} = \frac{1}{C}\left[\boldsymbol{I}_d(\boldsymbol{t})\boldsymbol{I}^{\mathbf{T}} - i_{\mathrm{ldv}}(t)\right] \tag{22}$$

where

$$\boldsymbol{U}_{\mathbf{in}} = \begin{bmatrix} U_{\mathrm{in}1} & 0 & \cdots & 0 \\ 0 & U_{\mathrm{in}2} & \cdots & 0 \\ \vdots & \vdots & \ddots & \vdots \\ 0 & 0 & \cdots & U_{\mathrm{in}n} \end{bmatrix}, \boldsymbol{L} = \begin{bmatrix} L_1 & 0 & \cdots & 0 \\ 0 & L_2 & \cdots & 0 \\ \vdots & \vdots & \ddots & \vdots \\ 0 & 0 & \cdots & L_n \end{bmatrix}.$$

Considering the current PI controller, (18) can be rewritten as

$$\begin{aligned} \frac{\boldsymbol{dD}_d(\boldsymbol{t})}{\boldsymbol{dt}} = &\left[-\frac{du_d(t)}{dt}\boldsymbol{I}\boldsymbol{R}^{-1} - \frac{\boldsymbol{dI}_d(\boldsymbol{t})}{\boldsymbol{dt}}\right]\boldsymbol{K}_{\mathbf{pi}} \\ &+ \left[-u_d(t)\boldsymbol{I}\boldsymbol{R}^{-1} - \boldsymbol{I}_d(\boldsymbol{t})\right]\boldsymbol{K}_{\mathbf{ii}} \end{aligned} \tag{23}$$

where

$$\boldsymbol{R} = \begin{bmatrix} r_1 & 0 & \cdots & 0 \\ 0 & r_2 & \cdots & 0 \\ \vdots & \vdots & \ddots & \vdots \\ 0 & 0 & \cdots & r_n \end{bmatrix}.$$

Substituting (21) and (22) into (23), (23) can be rewritten as

$$\begin{aligned} \frac{\boldsymbol{dD}_d(\boldsymbol{t})}{\boldsymbol{dt}} = &-\boldsymbol{I}_d(\boldsymbol{t}) \cdot \left(\frac{1}{C}\boldsymbol{I}^{\mathbf{T}}\boldsymbol{I}\boldsymbol{K}_{\mathbf{pi}}\boldsymbol{R}^{-1} + \boldsymbol{K}_{\mathbf{ii}}\right) \\ &- \boldsymbol{D}_d(\boldsymbol{t}) \cdot \boldsymbol{K}_{\mathbf{pi}}\boldsymbol{L}^{-1}\boldsymbol{U}_{\mathbf{in}} + u_d(t) \\ &\cdot \left(\boldsymbol{I}\boldsymbol{K}_{\mathbf{pi}}\boldsymbol{L}^{-1} - \boldsymbol{I}\boldsymbol{K}_{\mathbf{ii}}\boldsymbol{R}^{-1}\right) + i_{\mathrm{ldv}}(t) \cdot \frac{\boldsymbol{I}\boldsymbol{K}_{\mathbf{pi}}\boldsymbol{R}^{-1}}{C} \end{aligned} \tag{24}$$

where

$$\boldsymbol{K}_{\mathbf{pi}} = \begin{bmatrix} k_{\mathrm{pi}1} & 0 & \cdots & 0 \\ 0 & k_{\mathrm{pi}2} & \cdots & 0 \\ \vdots & \vdots & \ddots & \vdots \\ 0 & 0 & \cdots & k_{\mathrm{pi}n} \end{bmatrix},$$

$$\boldsymbol{K}_{\mathbf{ii}} = \begin{bmatrix} k_{\mathrm{ii}1} & 0 & \cdots & 0 \\ 0 & k_{\mathrm{ii}2} & \cdots & 0 \\ \vdots & \vdots & \ddots & \vdots \\ 0 & 0 & \cdots & k_{\mathrm{ii}n} \end{bmatrix}.$$

In order to analyze a general paralleled module system consisting of n converters, (21), (22), and (24) can be rewritten in a

$$\boldsymbol{A} = \begin{bmatrix} \mathbf{0} & \boldsymbol{L}^{-1}\boldsymbol{U}_{\mathbf{in}} & -\boldsymbol{L}^{-1}\boldsymbol{I}^{\mathbf{T}} \\ -\dfrac{\boldsymbol{K}_{\mathbf{pi}}\boldsymbol{R}^{-1}\boldsymbol{I}^{\mathbf{T}}\boldsymbol{I}}{C} - \boldsymbol{K}_{\mathbf{ii}} & -\boldsymbol{K}_{\mathbf{pi}}\boldsymbol{L}^{-1}\boldsymbol{U}_{\mathbf{in}} & \boldsymbol{K}_{\mathbf{pi}}\boldsymbol{L}^{-1}\boldsymbol{I}^{\mathbf{T}} - \boldsymbol{K}_{\mathbf{ii}}\boldsymbol{R}^{-1}\boldsymbol{I}^{\mathbf{T}} \\ \dfrac{1}{C} \cdot \boldsymbol{I} & \mathbf{0} & \mathbf{0} \end{bmatrix}$$

$$\boldsymbol{x} = \begin{bmatrix} \boldsymbol{I}_d(\boldsymbol{t}) & \boldsymbol{D}_d(\boldsymbol{t}) & u_d(t) \end{bmatrix}^{\mathbf{T}}, \ \boldsymbol{B} = \begin{bmatrix} \mathbf{0} & \dfrac{\boldsymbol{I}\boldsymbol{K}_{\mathbf{pi}}\boldsymbol{R}^{-1}}{C} & -\dfrac{1}{C} \end{bmatrix}^{\mathbf{T}}, \ \boldsymbol{y} = i_{\mathrm{ldv}}(t)$$

TABLE II
PARAMETERS FOR ANALYSIS AND EXPERIMENTAL SETUPS

	Parameters		Value
	Symbol	Description	
Electrical setup parameters	U_{in}	Input voltage	230 V
	L	Converter inductance	1.8 mH
	C	DC bus capacitance	8800 μF
Droop control parameters	r_1	VR of Converter 1	1 Ω
	r_2	VR of Converter 2	1/2 Ω
	r_3	VR of Converter 3	1/3 Ω
	r_4	VR of Converter 4	1/4 Ω
	U_{rate}	Rated bus voltage	100 V

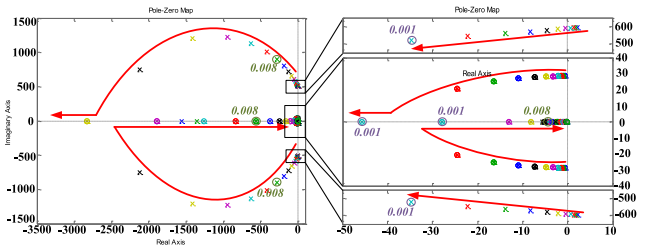

Fig. 8. Root locus analysis for all converters with proportional terms changing.

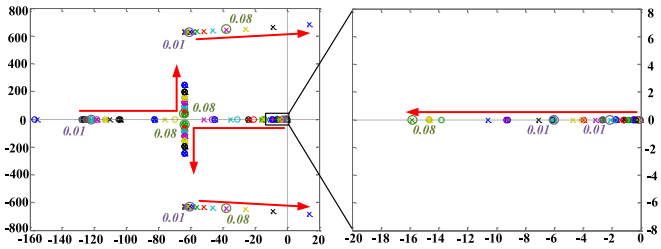

Fig. 9. Root locus analysis for all converters with integral terms changing.

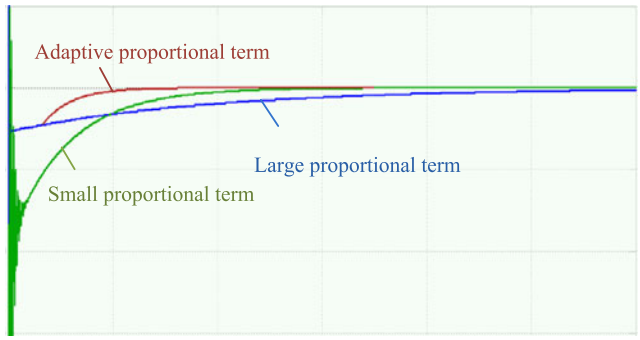

Fig. 10. Step response of output current under different proportional terms.

more compact state-space model defined as

$$\dot{\boldsymbol{x}} = \boldsymbol{A} \cdot \boldsymbol{x} + \boldsymbol{B} \cdot \boldsymbol{y} \tag{25}$$

where, see the equation shown at the bottom of the previous page.

In the state-space model, there are two state variables in each converter and one common state variable from the capacitor and load part. Thus, in the system with n converters, the total number of state variables is $(2n + 1)$. Taking four paralleled converters as an example, the root locus method is used based on the model shown in (25) to analyze the dynamic response of the system by shifting different control parameters. The electrical setup and VR parameters that are kept constant are shown in Table II.

The integral term values for four converters are initialized as 0.01, respectively. Then changing the proportional term values of all the converters from 0.00001 to 0.1, the pole shifting trajectories of all converters' average inductor currents are shown in Fig. 8, which demonstrates that appropriately increasing the proportional terms can decrease the fluctuations of converters' output currents and reduce part of the errors more rapidly during dynamical process. However, adverse effect on completely eliminating errors can be caused by increasing proportional terms. To be mentioned, the system can be unstable when all the proportional terms are too small.

When the four converters' proportional term values are initialized as 0.001, changing the integral term values of all the converters from 0.0001 to 1, respectively, the pole shifting trajectories of four converters' output currents can be observed as show in Fig. 9. According to the pole shifting trajectories, the result can be obtained that increasing integral terms can enlarge current fluctuations during dynamical process, but the errors can be eliminated more rapidly. Specifically, Fig. 9 shows that the system can be unstable when all the integral terms are too large.

B. Proposed Adaptive PI Control

According to the preceding analysis it can be seen that integral terms can be hardly optimized to improve the current sharing speed without fluctuations, so optimizing the proportional terms is the most effective way to improve the dynamic response performance. During dynamical process, the errors can be rapidly reduced by large proportional terms with no fluctuations and then completely eliminated under small proportional terms as shown in Fig. 10. In addition, the disturbances of duty ratios will be greater in steady state because of large proportional terms, which results in stronger fluctuating inductor currents against the steady-state characteristics [27]. Therefore, an adaptive PI controller with a compensator is proposed to improve the dynamic response of *I–V* droop control and guarantee good steady-state performance simultaneously.

Let $e_k(t)$ be the absolute error between current reference and average inductor current of the kth converter, then

$$e_k(t) = \left| -\frac{1}{r_k} u_d(t) - i_{dk}(t) \right|. \tag{26}$$

In steady state, the error between current reference and the average inductor current is zero, but during dynamical process, the error can be changed. When the $e_k(t)$ reaches the specific threshold value, the proportional term should be increased to improve the speed of error reduction. In steady state, let $\Delta u_{\max}$ represent the max fluctuation amplitude of the bus voltage ripple, $\Delta i_{\max k}$ represent the max ripple fluctuation amplitude of the average inductor current which is sampled by the kth

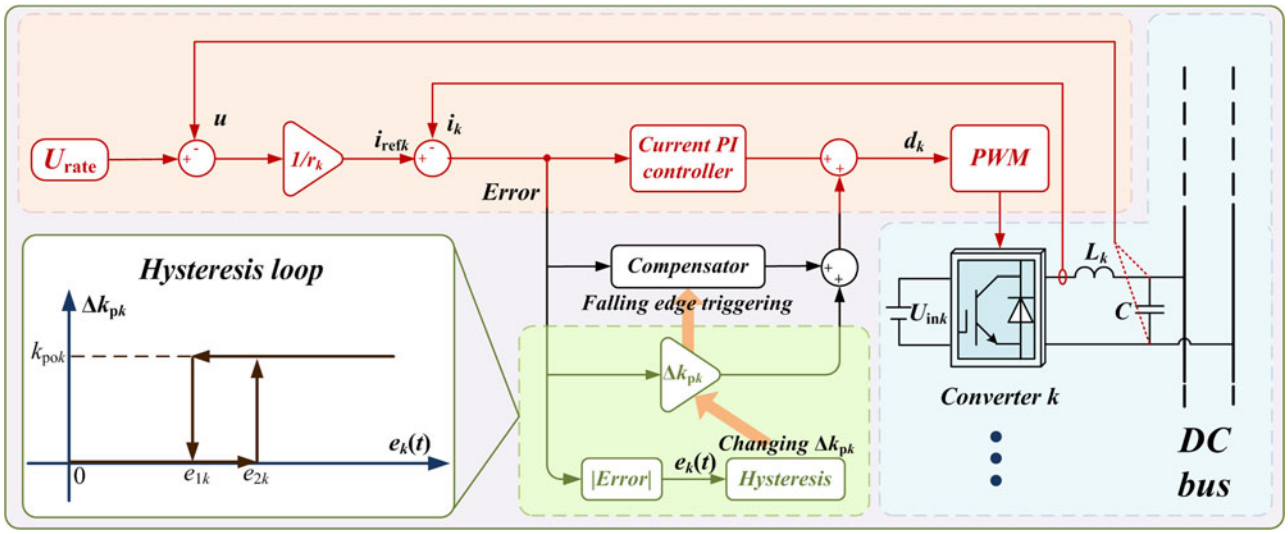

Fig. 11. Adaptive PI controller based on droop control.

converter. In order to guarantee the proportional term constant in steady state, this threshold value e_{1k} should satisfy the following condition as

$$e_{1k} > \frac{\Delta u_{\max}}{r_k} + \Delta i_{\max k}. \tag{27}$$

In order to prevent the frequent switching of the proportional term, the hysteresis loop needs to be used as shown in Fig. 11, so the follows can be obtained

$$\begin{cases} \Delta k_{\mathrm{p}k} = 0 & e_k(t) < e_{1k} \\ \Delta k_{\mathrm{p}k} = k_{\mathrm{po}k} & e_k(t) > e_{2k} \\ \Delta k_{\mathrm{p}k} \text{ is kept unchanging} & e_{1k} < e_k(t) < e_{2k} \end{cases} \tag{28}$$

where $\Delta k_{\mathrm{p}k}$ means the variation of proportional term of the kth converter, and $\Delta k_{\mathrm{p}k}$ needs to be increased to $k_{\mathrm{po}k}$ to improve the response speed when the absolute error increases to e_{2k}. As the absolute error is less than e_{1k}, $\Delta k_{\mathrm{p}k}$ returns to zero to eliminate the error rapidly and guarantee good stead-state performance. According to (3), the relationship between the n converters' threshold values can be obtained as

$$\begin{cases} e_{11} r_1 = e_{12} r_2 = \cdots = e_{1n} r_n \\ e_{21} r_1 = e_{22} r_2 = \cdots = e_{2n} r_n \\ e_{1k} > \Delta u_{\max}/r_k + \Delta i_{\max\, k} \qquad k = 1, 2, \ldots, n \end{cases}. \tag{29}$$

However, since the difference between the average inductor current and current reference is not always zero at the very beginning of $\Delta k_{\mathrm{p}k}$ restoring to zero, the output duty ratio of PI controller will change back at the falling edge of $\Delta k_{\mathrm{p}k}$ to induce that the output current returns back, which can increase $\Delta k_{\mathrm{p}k}$ to $k_{\mathrm{po}k}$ again. Since the above processes can take place repeatedly, fluctuations of currents will be induced and the dynamic can be weaker.

In order to solve this problem, the improved method for this adaptive PI controller is proposed. At the very beginning of $\Delta k_{\mathrm{p}k}$ restoring back, the output duty ratio needs to be constant to hold the inductor current, so a compensate term need to be added into the output duty ratio at the falling edge of $\Delta k_{\mathrm{p}k}$, which can be computed as

$$d_{\mathrm{cp}k} = k_{\mathrm{po}k} \left[i_{\mathrm{dref}k}(t) - i_{dk}(t) \right] \tag{30}$$

where $d_{\mathrm{cp}k}$ is the compensate value for the kth converter. Due to this improvement, the repeated fluctuations of currents can be avoided, and the voltage and current can smoothly transit from the dynamic process to the steady state. Thus, the dynamic response performances can be improved by the adaptive PI controller as shown in Fig. 11, and the steady characteristics can be guaranteed simultaneously.

C. Experiments of Adaptive PI Control

For the four converters whose parameters are listed in Table II, Fig. 8 shows that when all the integral term values are 0.01 and the proportional term values are not less than 0.001, there are no low-frequency fluctuating components, so that considering speeds of error elimination, the proportional term values can be initialized as 0.001. Putting into 350-W load, the bus voltage and four output currents are illustrated in Fig. 12 that shows that even though there are no oscillations, the transient response performances are slow.

The experiments have been performed by using the adaptive PI controller without the compensator. Fig. 8 shows that increasing proportional term values to 0.008, the speeds of error reduction can be obviously improved at the beginning of the dynamic process and all the fluctuating components can be further suppressed. Thus, initializing proportional and integral term values as 0.001 and 0.01, respectively, $k_{\mathrm{po}k}$ is set as 0.007. Putting into 350-W load, the bus voltage and four output currents are illustrated in Fig. 13, which shows that fluctuations of currents have been induced and transient response performances have not been enhanced.

With the compensator, the bus voltage and four output currents are illustrated in Fig. 14, which shows that the transient response performances have been obviously enhanced and the

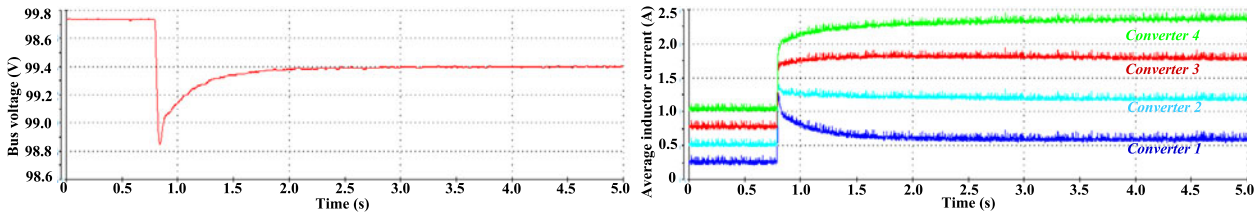

Fig. 12. Bus voltage and four output currents as $k_{\mathrm{pi}} = 0.001$ and $k_{\mathrm{ii}} = 0.01$.

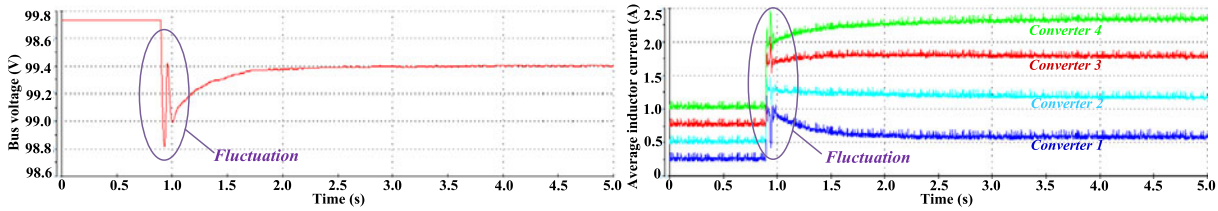

Fig. 13. Bus voltage and four output currents when the adaptive PI control is used without the compensator.

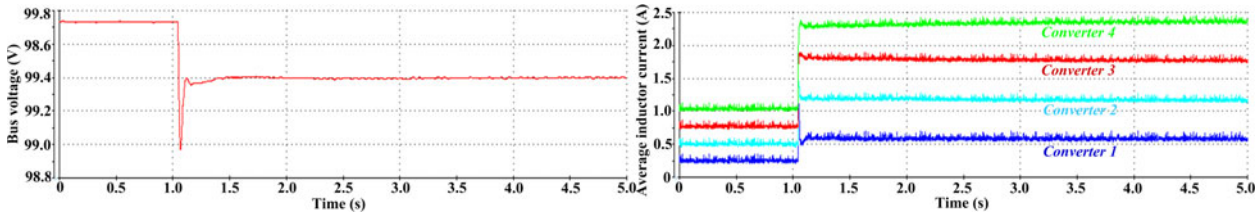

Fig. 14. Bus voltage and four output currents when the adaptive PI control is used with the compensator.

voltage sags are decreased as well. There are no huge oscillations or overshoots, and the voltage and current can smoothly transit from the dynamic process to the steady state. The experimental results verify that the dynamic characteristics can be significantly improved by using the proposed adaptive PI controller.

V. Conclusion

Two models considering *V–I* droop and *I–V* droop have been built separately, based on which this paper presents a dynamic response comparison between two droop controllers. The results show that the dynamic response performance of *I–V* droop control method is much faster than that of the *V–I* droop control because two more poles always exist near the imaginary axis in the *V–I* droop-based model no matter how to change the parameters. Furthermore, an adaptive PI controller with a duty ratio compensator is proposed to further improve the transient response performances of *I–V* droop controller. The compensate term of duty ratio is added into the control to hold output currents at the falling edge of proportional terms, which is indispensable for the realization of the proposed adaptive PI control. Experiments in a dc MG system have been performed to verify the effectiveness of the proposed control framework.

References

[1] M. Liserre, T. Sauter, and, Y. H. John, "Future energy systems: Integrating renewable energy sources into the smart power grid through industrial electronics," *IEEE Ind. Electron. Mag.*, vol. 4, no. 1, pp. 18–37, Mar. 2010.

[2] J. M. Carrasco *et al.*, "Power-electronic systems for the grid integration of renewable energy sources: A survey," *IEEE Trans. Ind. Electron.*, vol. 53, no. 4, pp. 1002–1016, Jul. 2006.

[3] D. D. C. Lu and V. G. Agelidis, "Photovoltaic-battery-powered DC bus system for common portable electronic devices," *IEEE Trans. Power Electron.*, vol. 24, no. 3, pp. 849–855, Feb. 2009.

[4] S. Anand and B. G. Fernandes, "Modified droop controller for paralleling of dc-dc converters in standalone dc system," *IET Power Electron.*, vol. 5, no. 6, pp. 782–789, Sep. 2012.

[5] R. Ahmadi and M. Ferdowsi, "Improving the performance of a line regulating converter in a converter-dominated DC microgrid system," *IEEE Trans. Smart Grid*, vol. 5, no. 5, pp. 2553–2563, Aug. 2014.

[6] T. Morstyn, B. Hredzak, and V. G. Agelidis, "Cooperative multi-agent control of heterogeneous storage devices distributed in a DC microgrid," *IEEE Trans. Power Syst.*, vol. 31, no. 4, pp. 2974–2986, Sep. 2015.

[7] X. Lu, K. Sun, J. M. Guerrero, J. C. Vasquez, L. Huang, and J. Wang, "Stability enhancement based on virtual impedance for DC microgrids with constant power loads," *IEEE Trans. Smart Grid*, vol. 6, no. 6, pp. 2770–2783, Aug. 2015.

[8] P. Wang, X. Lu, X. Yang, W. Wang, and D. Xu, "An improved distributed secondary control method for DC microgrids with enhanced dynamic current sharing performance," *IEEE Trans. Power Electron.*, vol. 31, no. 9, pp. 6658–6673, Nov. 2015.

[9] T. Dragičević, X. Lu, J. C. Vasquez, and J. M. Guerrero, "DC microgrids—Part I: A review of control strategies and stabilization techniques," *IEEE Trans. Power Electron.*, vol. 31, no. 7, pp. 4876–4891, Sep. 2015.

[10] A. P. N. Tahim, D. J. Pagano, E. Lenz, and V. Stramosk, "Modeling and stability analysis of islanded DC microgrids under droop control," *IEEE Trans. Power Electron.*, vol. 30, no. 8, pp. 4597–4607, Sep. 2014.

[11] Y. Fu *et al.*, "Research on power coordinated control strategy of wind turbine-based DC microgrid under various modes," in *Proc. 8th IEEE Power Electron. Motion Control Conf.*, 2016, pp. 1480–1484.

[12] X. Lu, J. M. Guerrero, K. Sun, and J. C. Vasquez, "An improved droop control method for dc microgrids based on low bandwidth communication with dc bus voltage restoration and enhanced current sharing accuracy," *IEEE Trans. Power Electron.*, vol. 29, no. 4, pp. 1800–1812, Jun. 2013.

[13] S. Augustine, M. K. Mishra, and N. Lakshminarasamma, "An improved droop control algorithm for load sharing and circulating current control for parallel DC-DC converters in standalone DC microgrid," in *Proc. 2014 Annu. Int. Conf. Emerg. Res. Areas: Magn., Mach. Drives*, 2014, pp. 1–6.
[14] Q. Zhong, "Robust droop controller for accurate proportional load sharing among inverters operated in parallel," *IEEE Trans. Ind. Electron.*, vol. 60, no. 4, pp. 1281–1290, Apr. 2011.
[15] S. Anand, B. G. Fernandes, and J. Guerrero, "Distributed control to ensure proportional load sharing and improve voltage regulation in low-voltage DC microgrids," *IEEE Trans. Power Electron.*, vol. 28, no. 4, pp. 1900–1913, Aug. 2012.
[16] S. Thomas, S. Islam, S. R. Sahoo, and S. Anand, "Distributed secondary control with reduced communication in low-voltage DC microgrid," in *Proc. 2016 10th Int. Conf. Compat., Power Electron. Power Eng.*, 2016, pp. 126–131.
[17] T. Dragičević, J. M. Guerrero, J. C. Vasquez, and D. Škrlec, "Supervisory control of an adaptive-droop regulated DC microgrid with battery management capability," *IEEE Trans. Power Electron.*, vol. 29, no. 2, pp. 695–706, Apr. 2013.
[18] X. Lu, K. Sun, J. M. Guerrero, J. C. Vasquez, and L. Huang, "Double-quadrant state-of-charge-based droop control method for distributed energy storage systems in autonomous DC microgrids," *IEEE Trans. Smart Grid*, vol. 6, no. 1, pp. 147–157, Sep. 2014.
[19] L. Meng, T. Dragicevic, J. Vasquez, J. Guerrero, and E. R. Sanseverino, "Hierarchical control with virtual resistance optimization for efficiency enhancement and state-of-charge balancing in DC microgrids," in *Proc. 2015 IEEE 1st Int. Conf. DC Microgrids*, 2015, pp. 1–6.
[20] L. Meng, T. Dragicevic, J. C. Vasquez, and J. M. Guerrero, "Tertiary and secondary control levels for efficiency optimization and system damping in droop controlled DC–DC converters," *IEEE Trans. Smart Grid*, vol. 6, no. 6, pp. 2615–2626, Nov. 2015.
[21] L. Meng, T. Dragicevic, J. M. Guerrero, and J. C. Vásquez, "Optimization with system damping restoration for droop controlled DC-DC converters," in *Proc. 2013 IEEE Energy Convers. Congr. Expo.*, 2013, pp. 65–72.
[22] L. Meng, T. Dragicevic, J. M. Guerrero, and J. C. Vasquez, "Dynamic consensus algorithm based distributed global efficiency optimization of a droop controlled DC microgrid," in *Proc. 2014 IEEE Int. Energy Conf.*, 2014, pp. 1276–1283.
[23] L. Meng, T. Dragicevic, J. Roldán-Pérez, J. C. Vasquez, and J. M. Guerrero, "Modeling and sensitivity study of consensus algorithm-based distributed hierarchical control for DC microgrids," *IEEE Trans. Smart Grid*, vol. 7, no. 3, pp. 1504–1515, May 2016.
[24] T. Dragičević, X. Lu, J. C. Vasquez, and J. M. Guerrero, "DC microgrids—Part II: A review of power architectures, applications, and standardization issues," *IEEE Trans. Power Electron.*, vol. 31, no. 5, pp. 3528–3549, May 2016.
[25] K. Yu, Q. Ai, S. Wang, J. Ni, and T. Lv, "Analysis and optimization of droop controller for microgrid system based on small-signal dynamic model," *IEEE Trans. Smart Grid*, vol. 7, no. 2, pp. 695–705, Mar. 2016.
[26] J. Leppäaho and T. Suntio, "Dynamic characteristics of current-fed super-buck converter," *IEEE Trans. Power Electron.*, vol. 26, no. 1, pp. 200–209, Jan. 2011.
[27] H. Wang, M. Han, W. Yan, G. Zhao, and J. M. Guerrero, "A feed-forward control realizing fast response for three-branch interleaved DC-DC converter in DC microgrid," *Energies*, vol. 9, no. 7, Jul. 2016, Art. no. 529.
[28] B. Oraw and R. Ayyanar, "Large signal average model for an extended duty ratio and conventional buck," in *Proc. 2008 IEEE 30th Int. Telecommun. Energy Conf.,* 2008, pp. 1–8.
[29] S. Chiniforoosh *et al.*, "Definitions and applications of dynamic average models for analysis of power systems," *IEEE Trans. Power Del.*, vol. 25, no. 4, pp. 2655–2669, Oct. 2010.
[30] V. Vorperian, "Simplified analysis of PWM converters using model of PWM switch. II. Discontinuous conduction mode," *IEEE Trans. Aerosp. Electron. Syst.*, vol. 26, no. 3, pp. 497–505, May 1990.
[31] G. Nirgude, R. Tirumala, and N. Mohan, "A new, large-signal average model for single-switch DC-DC converters operating in both CCM and DCM," in *Proc. 2001 IEEE 32nd Annu. Power Electron. Spec. Conf. (IEEE Cat. No.01CH37230),* 2001, pp. 1736–1741.
[32] J. Sun, "Unified averaged switch models for stability analysis of large distributed power systems," in *Proc. 15th Annu. IEEE Appl. Power Electron. Conf. Expo. (Cat. No.00CH37058)*, vol. 1, 2000, pp. 249–255.
[33] T. Pavlovic, T. Bjazic, and Z. Ban, "Simplified averaged models of DC–DC power converters suitable for controller design and microgrid simulation," *IEEE Trans. Power Electron.*, vol. 28, no. 7, pp. 3266–3275, Jul. 2013.
[34] S. Chiniforoosh *et al.*, "Definitions and applications of dynamic average models for analysis of power systems," *IEEE Trans. Power Del.*, vol. 25, no. 4, pp. 2655–2669, Oct. 2010.
[35] S. Liu, L. Zhou, and W. Lu, "Simple analytical approach to predict large-signal stability region of a closed-loop boost DC–DC converter," *IET Power Electrons*., vol. 6, no. 3, pp. 488–494, Mar. 2013.
[36] C. T. Chen, S. T. Peng, and C. Hwang, "A direct adaptive PI control scheme for process control," in *Proc. 2007 Eur. Control Conf.*, 2007, pp. 5839–5844.
[37] R. M. Milasi and M. Moallem, "Adaptive PI control of a three phase AC/DC PWM converter," in *Proc. 40th Annu. Conf. IEEE Ind. Electron. Soc.*, 2014, pp. 65–70.
[38] M. Hernandez-Gomez, R. Ortega, F. Lamnabhi-Lagarrigue, and G. Escobar, "Adaptive PI stabilization of switched power converters," *IEEE Trans. Control Syst. Technol.*, vol. 18, no. 3, pp. 688–698, May 2010.

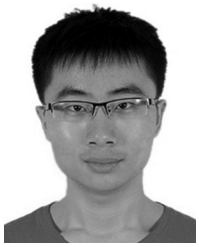

Haojie Wang (S'16) was born in Henan, China, in 1989. He received the B.S. degree in electrical engineering and automation from Zhengzhou University, Zhengzhou, China, in 2013. He is currently working toward the Ph.D. degree in power system and automation at North China Electric Power University, Beijing, China.

He is currently a guest Ph.D. student in the Department of Energy Technology, Aalborg University, Aalborg, Denmark. His research interests include power electronics, control, and their applications in dc microgrids.

Minxiao Han was born in Shannxi, China, in 1963. He received the Ph.D. degree in electrical engineering and automation from North China Electric Power University (NCEPU), Beijing, China, in 1995.

He was a visiting Ph.D. student with Queen's University of Belfast, U.K., and a Postdoctoral Fellow with Kobe University, Japan. He is currently the Director of Institute of Flexible Electric Power Technology, NCEPU. He has been the leader in projects consigned by National Nature Science Foundation of China, National Educational Ministry, and enterprises. He has four published books and more than 100 refereed publications in journals and conferences. His research interests are the applications of power electronics in power system including HVdc, FACTS, and power conversion and control.

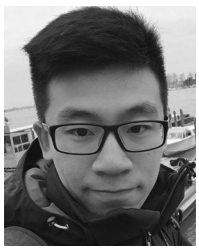

Renke Han (S'16) was born in Anshan, China, in 1991. He received the B.S. degree in automation, the M.S. degree in control theory and control engineering, both from Northeastern University, Shenyang, China, in 2013 and 2015, respectively. He is currently working toward the Ph.D. degree in microgrid in the Department of Energy Technology, Aalborg University, Aalborg, Denmark.

He is currently a guest Ph.D. student with Laboratoire d'Automatique, Ecole polytechnique fédérale de Lausanne, Lausanne, Switzerland, under the supervision of Prof. Giancarlo Ferrari-Trecate. His research interests include the distributed control, event-triggered control, plug-and-play control to achieve stability operation, and reasonable power sharing for ac and dc microgrid.

Josep M. Guerrero (S'01–M'04–SM'08–F'15) received the B.S. degree in telecommunications engineering, the M.S. degree in electronics engineering, and the Ph.D. degree in power electronics from the Technical University of Catalonia, Barcelona, Spain, in 1997, 2000, and 2003, respectively.

Since 2011, he has been a Full Professor in the Department of Energy Technology, Aalborg University, Aalborg, Denmark, where he is responsible for the Microgrid Research Program (www.microgrids.et.aau.dk). Since 2012, he has been a Guest Professor at the Chinese Academy of Science, Beijing, China, and the Nanjing University of Aeronautics and Astronautics, Nanjing, China; since 2014, he has been a Chair Professor in Shandong University, Jinan, China; since 2015, he has been a Distinguished Guest Professor in Hunan University, Changsha, China; and since 2016, he has been a Visiting Professor Fellow at Aston University, Birmingham, U.K., and a Guest Professor at the Nanjing University of Posts and Telecommunications, Nanjing, China. His research interests is oriented to different microgrid aspects, including power electronics, distributed energy-storage systems, hierarchical and cooperative control, energy management systems, smart metering and the internet of things for ac/dc microgrid clusters and islanded minigrids; recently specially focused on maritime microgrids for electrical ships, vessels, ferries, and seaports.

Prof. Guerrero is an Associate Editor for the IEEE TRANSACTIONS ON POWER ELECTRONICS, the IEEE TRANSACTIONS ON INDUSTRIAL ELECTRONICS, and the IEEE INDUSTRIAL ELECTRONICS MAGAZINE, and an Editor for the IEEE TRANSACTIONS ON SMART GRID, and the IEEE TRANSACTIONS ON ENERGY CONVERSION. He has been the Guest Editor of the IEEE TRANSACTIONS ON POWER ELECTRONICS Special Issues: Power Electronics for Wind Energy Conversion and Power Electronics for Microgrids; the IEEE TRANSACTIONS ON INDUSTRIAL ELECTRONICS Special Sections: Uninterruptible Power Supplies systems, Renewable Energy Systems, Distributed Generation and Microgrids, and Industrial Applications and Implementation Issues of the Kalman Filter; the IEEE TRANSACTIONS ON SMART GRID Special Issues: Smart DC Distribution Systems and Power Quality in Smart Grids; the IEEE TRANSACTIONS on ENERGY CONVERSION Special Issue on Energy Conversion in Next-generation Electric Ships. He was the Chair of the Renewable Energy Systems Technical Committee of the IEEE Industrial Electronics Society. He received the Best Paper Award of the IEEE TRANSACTIONS ON ENERGY CONVERSION for the period 2014–2015, and the Best Paper Prize of IEEE-PES in 2015. He also received the Best Paper Award of the *Journal of Power Electronics* in 2016. In 2014, 2015, and 2016, he received the Highly Cited Researcher by Thomson Reuters, and in 2015, he was elevated as the IEEE Fellow for his contributions on "Distributed power systems and microgrids."

Juan C. Vasquez (M'12–SM'14) received the B.S. degree in electronics engineering from the Autonomous University of Manizales, Manizales, Colombia, and the Ph.D. degree in automatic control, robotics, and computer vision from the Technical University of Catalonia, Barcelona, Spain, in 2004 and 2009, respectively.

He was with the Autonomous University of Manizales working as a teaching assistant and the Technical University of Catalonia as a Postdoctoral Assistant in 2005 and 2008, respectively. In 2011, he was an Assistant Professor and since 2014, he has been working as an Associate Professor in the Department of Energy Technology, Aalborg University, Aalborg, Denmark, where he is currently the Vice Programme Leader of the Microgrids Research Program (see microgrids.et.aau.dk). From February 2015 to April 2015, he was a visiting scholar at the Center of Power Electronics Systems at Virginia Tech and a Visiting Professor at Ritsumeikan University, Kyoto, Japan. He has authored and coauthored more than 100 technical papers only in microgrids in international IEEE conferences and journals. His current research interests include operation, advanced hierarchical and cooperative control, optimization and energy management applied to distributed generation in ac/dc microgrids, maritime microgrids, advanced metering infrastructures, and the integration of Internet of Things and cyber-physical systems into the SmartGrid.

Dr. Vasquez is an Associate Editor of IET Power Electronics. He is currently a member of the IEC System Evaluation Group SEG4 on LVdc distribution and safety for use in developed and developing economies, the Renewable Energy Systems Technical Committee TC-RES in the IEEE Industrial Electronics, PELS, IAS, and PES Societies.